Chemical Engineering Journal 489 (2024) 151088

Contents lists available at ScienceDirect

Chemical Engineering Journal

journal homepage: www.elsevier.com/locate/cej

Post-discharge: An interesting step to improve heterogeneous catalysts synthesized by glidarc plasma?

F. Hanon, E.M. Gaigneaux *

Institute of Condensed Matter and Nanosciences (IMCN), Université catholique de Louvain (UCLouvain), Place Louis Pasteur 1, 1348 Louvain-la-Neuve, Belgium

ARTICLE INFO

Keywords:
Glidarc plasma
Post-discharge
Catalysts
(hydr)oxides
Precipitation
Maturation

ABSTRACT

Gliding arc plasma (GP) is an interesting method for the synthesis of heterogeneous catalysts. In this process, precursors (metal salts) undergo a reaction with plasma species, resulting in the formation of a precipitate. Previous literature documents the synthesis of catalysts such as FeO_x and MnO_x derived from $(NH_4)_2Fe(SO_4)_2$ and $KMnO_4$, revealing that incorporating a post-discharge (PD) step can introduce valuable properties like phase transformation, increased specific surface area and enhanced catalytic activity. Hypotheses have been proposed to explain the changes that the solids undergo during this step, suggesting that the long-lived species created in PD influence the solids transformation. However, no conclusive evidence supporting these hypotheses has been provided. Therefore, the aim of the research presented here is to explore the influence of PD on various types of solids synthesized by GP and to understand the underlying mechanisms of this step. To investigate the role of PD, we exposed iron and tin precursors to the plasma, and submitted them to two types of PD. The respective synthesis conditions do not consistently impact the characteristics of the plasma-synthesized solids for the different metals. However, a common pattern emerges when examining the influence of the PD on different salts of a given metal. Specifically, solids obtained from different precursors of the same metal, identically exhibit superior catalytic activity when synthesized under similar conditions. To understand the mechanism underlying the PD step and investigate the hypothesis that the long-lived species created in PD influence the solids transformation, we exposed iron and tin precursors to a PD where no plasma species were present. To do so, the plasma-synthesized solids were recovered and placed into pure distilled water before performing the PD step. This enables a comparison of the solids obtained under these conditions with those obtained through classical PD, where plasma species are present. We understood that, even though long-lived plasma species present during the PD can still trigger the reaction of metal ions remaining in solution, they do not impact the way the solid is transformed during this stage.

1. Introduction

Due to their significant impact on economic and environmental indicators of industrial processes, catalysts are used in 85–90 % of chemical industries [1–3]. Given the increasing importance of these criteria in today's context, there is a growing emphasis on the development of new synthesis methods and the production of catalysts with interesting characteristics such as selectivity, activity, stability, mechanical and thermal resistance, recyclability, and cost-effectiveness [1,4–6]. Consequently, research efforts are continuously focused on discovering and enhancing catalysts properties and synthesis.

In this context, gliding arc (glidarc) plasma (GP) technology appears as a promising technique (Fig. 1). The glidarc plasma reactor, initially conceived by H. Lesueur and later refined by A. Czernichowski in 1988, consists of two stainless steel electrodes with a divergent profile connected to a high voltage generator [7,8]. Upon activation of the generator, an arc is formed at the narrowest distance between the electrodes. Simultaneously, a flow of gas (hereafter named plasma gas) is sent perpendicular to the arc, causing it to glide along the electrodes. As the electrodes diverge at their ends, the arc breaks due to the increased distance, leading to the formation of a new arc (Fig. 1). In this system, the arc, which constitutes the thermal part of the plasma, is cooled down to nearly ambient temperature through the gliding process and bursts into a plume of quenched plasma at atmospheric pressure [7,9–14].

The plasma plume contains various species, including electrons, cations, and free radicals, among others. These highly reactive

* Corresponding author.
E-mail address: eric.gaigneaux@uclouvain.be (E.M. Gaigneaux).

https://doi.org/10.1016/j.cej.2024.151088
Received 5 February 2024; Received in revised form 15 March 2024; Accepted 7 April 2024
Available online 8 April 2024

components can be harnessed for achieving chemical reactions within and/or on gas, solid, or liquid targets. Particularly, when humid air is employed as plasma gas, the generated "reactive oxygen and nitrogen species" (RONS) are known to predominantly exhibit acidic and oxidant effects on the target (Fig. 1). These characteristics have led to the application of GP in various fields, such as gas depollution or valorization, wastewater treatment, surface modification of solid materials, and the synthesis of heterogeneous catalysts [14–20].

This method has already demonstrated its potential for synthesizing metal (hydr)oxides (TiO_2, FeO_x, MnO_2, SnO_2) and supported catalysts (FeO_x/Kaolinite, TiO_2/SnO_2). These materials exhibit excellent properties and catalytic activity when used for pollutant degradation in both gaseous and liquid phases (Table 1) [15–17,21–24]. Moreover, GP offers interesting conditions when compared to alternative synthesis methods. One of the most significant advantages is the mild conditions and short processing time it requires. Additionally, this approach can be considered eco-friendly and cost-effective, as the only chemical used to generate these reactive species is water-saturated air, which is non-polluting, available, and renewable [15].

For some previously synthesized catalysts documented in the literature, such as FeO_x and MnO_x derived from $(NH_4)_2Fe(SO_4)_2$ and $KMnO_4$ through GP exposure, it has been observed that implementing a post-discharge (PD) step in their synthesis can impart valuable new properties such as phase transformation, increased specific surface area, and enhanced catalytic activity (Table 2, Fig. 1) [15,27].

The PD step consists of, after exposing the precursor solution to GP and turning off the discharge, allowing the solution to stand outside the reactor for a defined duration and at a fixed temperature. Hypotheses have been proposed to explain the changes that the solid undergoes during this step, suggesting that the long-lived species created in PD might influence the solid's transformation. However, no conclusive evidence supporting these hypotheses has been provided. At this stage, this step is clearly not fully understood. Therefore, it remains challenging to determine *a priori* whether it is beneficial to incorporate the PD step in the glidarc plasma synthesis of various catalysts.

Given this context, the aim of the research presented here was to explore the influence of PD on various types of solids synthesized by GP and to understand the underlying mechanisms of this step. This investigation was undertaken with the purpose of gaining a more comprehensive understanding of the synthesis of catalysts by GP, aiming to refine and improve the process. This goal aligns with the broader objective of developing interesting catalysts through this innovative, economically viable, and environmentally friendly approach. Here, we particularly focus on the synthesis of catalysts dedicated to air

Table 1
Hypothetical reactions during catalysts syntheses by humid air glidarc plasma evoked in the literature.

Precursor	Catalyst synthesized	Synthesis reaction
$TiCl_3$	TiO_2 [17,25]	$TiCl_3 + OH^{\cdot} + H_2O \rightarrow TiO_2 + 3HCl$
$TiCl_3 + SnCl_2{\cdot}2H_2O$	TiO_2/SnO_2 [21]	$TiCl_3 + SnCl_2 + 3OH^{\cdot} + H_2O \rightarrow TiO_2/SnO_2 + 5HCl$
$(NH_4)_2Fe(SO_4)_2{\cdot}6H_2O$	FeOOH [15]	(1) $Fe^{2+} + OH^{\cdot} \rightarrow Fe^{3+} + OH^{-}$ (2) $Fe^{3+} + 2OH^{-} + H_2O \rightarrow FeOOH + H_3O^{+}$
	Fe_2O_3 [15]	$2FeOOH \xrightarrow{calcination} Fe_2O_3 + H_2O$
Mayouom Kaolinite + $(NH_4)_2Fe(SO_4)_2{\cdot}6H_2O$	FeO_x/kaolinite [26]	(1) $Fe^{2+} + OH^{\cdot} \rightarrow Fe^{3+} + OH^{-}$ (2) $Fe^{3+} + 2OH^{-} + H_2O \rightarrow FeOOH + H_3O^{+}$
$KMnO_4$	α-MnO_2 and γ-MnO_2 [16,24]	$MnO_4^{-} + NO^{\cdot} \rightarrow MnO_2 + NO_3^{-}$
$Mn(CH_3COO)_3{\cdot}2H_2O$	γ-MnO_2 and β-MnO_2 [24]	$Mn^{3+} + OH^{\cdot} + H_2O \rightarrow MnO_2 + H^{+}$
$SnCl_2$	SnO_2 [21]	(1) $SnCl_2 + H_2O \leftrightarrow Sn(OH)Cl + HCl$ (2) $Sn(OH)Cl + 3OH^{\cdot} \rightarrow SnO_2 + 2H_2O + \frac{1}{2}Cl_2$

Table 2
Effect of the post-dicharge step at 100 °C and/or 25 °C on solids synthesized from $(NH_4)_2Fe(SO_4)_2$ and $KMnO_4$ (compilation of [15,27]).

	$(NH_4)_2Fe(SO_4)_2$	$KMnO_4$	
	PD at 100 °C (1,2,3h)	**PD at 100 °C (1,2,3h)**	**PD at 25 °C (24,48,72 h)**
Change of phase	Amorphous solid → crystalline α-FeOOH	α-MnO_2 → γ-MnO_2	
Specific surface area	↗	↘	↗
Pore volume	↗	↘	↗
Catalytic activity	↗	↘	↗

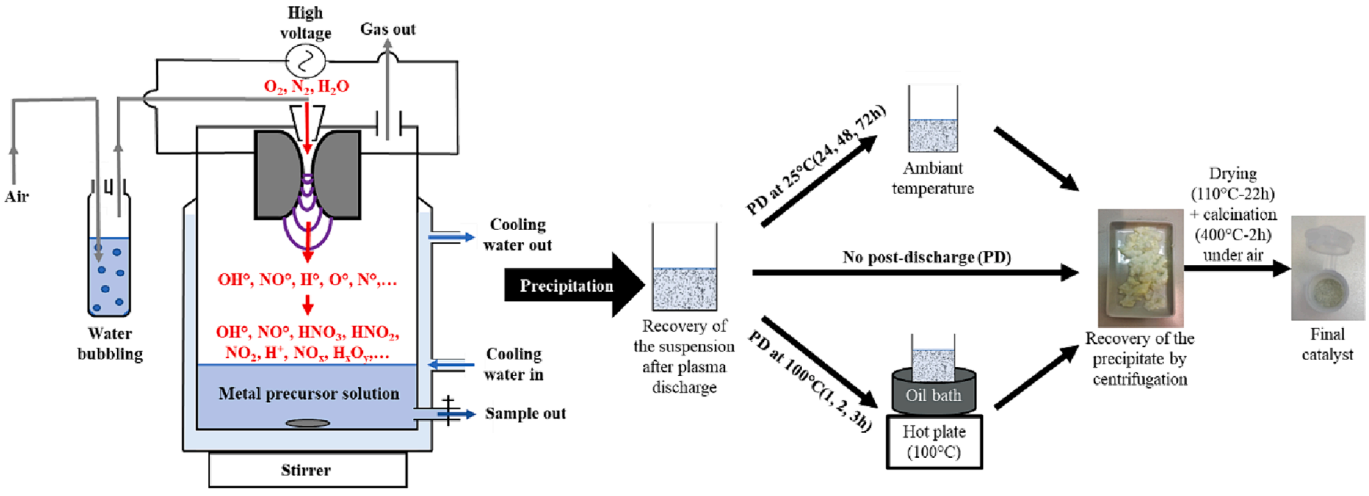

Fig. 1. Scheme of glidarc plasma reactor, species mainly present in a humid air glidarc plasma [14] and scheme of catalysts synthesis with and without a post-discharge step.

depollution by the total oxidation of pollutants.

2. Experimental methods

2.1. Materials

Iron(II) sulfate heptahydrate ($FeSO_4·7H_2O$; ≥ 99 %), tin(II) sulfate ($SnSO_4$; ≥ 95 %) and tin(II) chloride ($SnCl_2$; ≥ 99 %) were purchased from Sigma Aldrich and ammonium-iron(II) sulfate hexahydrate ($(NH_4)_2Fe(SO_4)_2·6H_2O$; ≥ 99 %) from Roth.

2.2. Method

2.2.1. Synthesis device: The GP reactor

The gliding arc plasma system employed in this study comprises the following components (Fig. 1):

- A high voltage generator (ABL Transformer; 9 kV; 100 mA) connected to both stainless-steel electrodes with a divergent profile, positioned within the reactor.
- A gas supply setup consists of a compressed air source, a saturator filled with water in which air is bubbled, and a flowmeter controlling the gas flow rate (fixed at ≈ 400 L/h).
- A central reactor in the form of a double-walled cylindrical glass tube. It features inlets and outlets for the circulation of an external cooling fluid (water), an additional inlet for the nozzle to direct the air flow between the electrodes, and an opening for the gas exhaust (to prevent exceeding pressure within the reactor). An outlet valve is also present to facilitate retrieval of the reactor content following plasma exposure.

2.2.1.1. Materials synthesis. The precursor solutions were prepared by dissolving these compounds in deionized water. Subsequently, 450 mL of the respective solutions were introduced into the reactor, stirred magnetically (1 rotation/s), and exposed to the plasma discharge for 45 min for $(NH_4)_2Fe(SO_4)_2·6H_2O$, 60 min for $FeSO_4·7H_2O$ and 120 min for $SnSO_4·7H_2O$ and $SnCl_2$.

To investigate the impact of the PD on different types of solids, 2 recovery methods were performed:

- For catalysts produced without PD (named “no PD”), the solid formed when the solution is exposed to the plasma discharge was recovered by centrifugation (24490G, 30 min) and subjected to two washing cycles with distilled water.
- For catalysts produced with PD, the suspension obtained after plasma exposure was collected and placed in a berlin before undergoing the PD step. The PD was conducted in 2 different ways: by allowing the berlin to stand at room temperature (≈25 °C) for 72 h (named “+ PD (72 h-25 °C)”) or by immersing it in an oil bath at 100 °C for 3 h (named “+ PD (3 h-100 °C)”). The resulting solid was then recovered through centrifugation (24490G, 30 min) and subjected to two washing cycles with distilled water.

Blanks were prepared for each precursor to assess the influence of plasma on their reaction. For the precursor exposed to plasma without PD, solution precursor was stirred at ambient temperature for the same duration as during normal exposure to the glidarc (named “name of the precursor no plasma”). For the solids subjected to a PD step, after ambient temperature stirring, the solution/suspension was transferred in a berlin before undergoing a “PD” at 25 °C for 72 h (named “+ PD (72 h-25 °C) no plasma”) or at 100 °C for 3 h (named “+ PD (3 h-100 °C) no plasma”). If a precipitate formed, it was recovered, washed, and dried, as for the solids formed by glidarc plasma.

To understand the mechanism underlying the PD step, a comparative analysis was conducted between the solids derived from $(NH_4)_2Fe(SO_4)_2$ and $SnSO_4$ when subjected to a classical PD and a PD performed without plasma species present in the system (named “+ PD (72 h-25 °C) new water” or “+ PD (3 h-100 °C) new water”). The process involved recovering the precipitate after the plasma discharge through centrifugation at 24490G for 30 min. Subsequently, a new suspension was created by placing the precipitate in 450 mL of pure distilled water. This suspension was then transferred to a berlin undergoing the PD either at room temperature (≈25 °C) for 72 h or in an oil bath at 100 °C for 3 h.

All the solids obtained after centrifugation were dried in an oven under air at 110 °C for 22 h ± 2 h and then calcined in a muffle furnace under air at 400 °C for 2 h.

The samples are referenced as follows: “Name of the precursor – synthesis conditions (no PD; + PD (3 h-100 °C); + PD (72 h-25 °C); + PD (3 h-100 °C) new water; + PD (72 h-25 °C) new water))”.

2.3. Characterization of the solids formed

All the characterizations presented here were done after the calcination of the solids formed, except for the XRD that was done before and after the calcination step.

2.3.1. X-ray diffraction (XRD)

The catalyst, previously ground, is placed on a polished Si single crystal sample holder covered with a thin layer of Nivea© cream and is introduced into a Bruker-D8 Advance diffractometer with a Bragg-Brentano geometry. The X-rays sent to the sample are produced using a copper anode (Kα = 0.15418 nm). The analysis is performed for angles 2θ = 5° to 80° with an increment of 0.015° and 0.15 s integration time. Detection is performed using a LynxEye XE-T Technology detector. The diffractograms are then processed using the ICDD-PDF2-2004 database [28].

2.3.2. X-ray photoelectron spectroscopy (XPS)

The samples, previously crushed, are placed on a double-sided sticker, which is itself placed on a 4 mm diameter stainless steel sample holder placed in an aluminum carousel. The samples are then degassed under ultra-high vacuum at 10^{-5} Pa for 12 h in order to eliminate the physisorbed compounds before being analyzed. The machine used is an SSX 100/206 Photoelectrons Spectrometer from Surface Science Instruments (USA). It is equipped with a micro-focused monochromatic Al X-ray source powered at 20 mA and 10 kV. The pressure inside the analysis chamber is 10^{-8} Pa, and the analysis angle is 55°. An electron gun operating at 8 eV and a Ni grid placed 3 mm above the sample surface are used to ensure that the sample charge is stabilized during analysis. The data are processed using the CasaXPS program from Casa Software Ltd, UK. To calibrate the binding energy, the C-(C,H) component of the C 1 s peak is positioned at 284.8 eV. The spectra can then be decomposed, and the atomic percentages are obtained using the normalized peak areas, the sensitivity factors provided by the manufacturer, and a Shirley-type baseline. The atomic percentages of each element are recalculated by removing the carbon contamination due to the experimentation. From the percentage obtained for O 1 s, the quantity of O atoms bound to the carbon contamination is deduced, considering 3 types of carbon–oxygen bonds: O-C = O; O-C-O and C = O; C-O. The remaining percentages of the elements not coming from the contamination are then brought back to 100 %.

2.3.3. Scanning electron microscopy (SEM) and energy dispersive X-ray (EDX)

The ground solids are placed on an adhesive carbon film, which is itself deposited on an aluminum support. The scanning electron microscope used is a JEOL 7600F operating at 2 kV for the SEM images in GBH mode and at 15 kV for the EDX analyses. The atomic percentages of each element are recalculated by removing carbon and aluminum contamination. All remaining percentages are then brought back to 100 %.

2.3.4. N_2-physisorption

N_2-physisorption is used to measure the specific surface area by the BET method (Brunauer, Emmet, and Teller) and the pore volume by the BJH method (Barret-Joyner-Halenda). In practice, the weighed ground solids are introduced into glass tubes with a filler rod to limit the error in the measurement due to the dead volume of the glass tubes. A vacuum degassing of at least 6 h at 140 °C is carried out at a vacuum of approximately 10 mbar. After degassing, the powder is weighed again. Then the glass tube is introduced into a specific surface and porosity analyzer (TriStar from Micromeritics). The analysis is carried out using nitrogen at −196 °C in the range of relative pressures from 0.01 to 0.99.

2.3.5. Catalytic test

The catalytic activity of the synthesized solids is tested by comparing their ability to totally oxidize benzene in the gas phase at different temperatures (Eq. (1)).

$$C_6H_6 + \frac{15}{2}O_2 \rightarrow 6CO_2 + 3H_2O \quad (1)$$

The catalysts tested are sieved to achieve a particle size ranging between 200 and 315 µm. A constant mass of 100 mg of catalyst, mixed with 400 mg of glass beads measuring between 350 and 500 µm, is introduced into the reactor between 2 layers of quartz wool so that the catalyst occupies a uniform volume within the reactor. The reaction gas, containing 200 ppm by volume of benzene and 10 vol% O_2, is continuously supplied to the reactor at a flow of 100 mL/min throughout the analysis, with He serving as the carrier gas. The reagent-to-catalyst volume ratio per hour (VVH) is maintained at approximately 60000 h^{-1}. The reactor operates within a temperature range from 50 to 400 °C, with increments of 50 °C per stage. At the outlet of the reactor, the gas effluent is directed to a Varian CP-3800 gas chromatograph equipped with a CP-sil 8CB column and a flame ionization detector (FID). He is used as the GC carrier gas and the analysis is conducted at a constant temperature of 80 °C. To calculate the remaining (not converted) benzene, four injections of the reactor outlet gas are performed for each tested temperature.

Calibration is performed based on the benzene peak. It is assumed that at the initial reactor temperature, i.e. 50 °C, benzene does not undergo any conversion, and the peak area at this temperature signifies 0 % conversion. Using this reference area, the benzene conversion for each temperature stage is calculated using an equation of the following form (Eq. (2)):

$$\frac{peak\ area\ at\ 50^{\circ}C - peak\ area\ at\ a\ given\ temperature}{peak\ area\ at\ 50^{\circ}C} * 100 \quad (2)$$

3. Results and discussion

3.1. Investigation of the impact of the PD

3.1.1. Iron precursors

Table 3 shows the amount of solid recovered after iron precursors were exposed to the plasma, without and with a PD under different conditions. The plasma indeed influences the reaction of iron precursors, as without plasma-generated species, the precursors do not spontaneously precipitate. This implies that the species formed through glidarc plasma have the ability to react with the precursors, leading to a subsequent precipitate. Moreover, the increased amount of recovered solid for both types of PD (3 h-100 °C and 72 h-25 °C) shows that this step enables the species created during the plasma discharge to persist in their reactivity, allowing further precipitation. Furthermore, as the duration of the PD time increases (between 3 h and 72 h), the quantity of solid recovered also increases (Table 3). The quantification analysis, by UV–visible spectroscopy, of Fe^{2+} ions from the precursors remaining in solution after exposure and PD confirmed a progressive increase in the formation of solids during the PD step (Supplementary information SI.1).

Table 3
Mass of solid produced and pH of the solution when iron precursors are exposed to the glidarc plasma without PD, with PD (3 h-100 °C and 72 h-25 °C) and without plasma.

	Mass of solid produced (g)		pH		
	After exposure/ PD	After no plasma exposure	Precursor solution	After exposure	After PD
$(NH_4)_2Fe(SO_4)_2$ no PD	0.050	0			/
$(NH_4)_2Fe(SO_4)_2$ + PD (3 h-100 °C)	0.119	0			1.9
$(NH_4)_2Fe(SO_4)_2$ + PD (72 h-25 °C)	0.177	0	4	3	2.6
$FeSO_4$ no PD	0.131	0			/
$FeSO_4$ + PD (3 h-100 °C)	0.152	0			2.7
$FeSO_4$ + PD (72 h-25 °C)	0.242	0			2.6

As a result of the formation of H^+ species by plasma, the medium gets acidified during the exposure process (Table 3). Throughout the PD, the pH continues to decrease due to the ongoing formation of H^+ species, originating from HNO_3 and HNO_2 [14].

XRD diffractograms of the solids generated from the iron precursors reveal that the phases developed, whatever the synthesis type are approximately the same (Fig. 2). Both $(NH_4)_2Fe(SO_4)_2$ and $FeSO_4$ no PD consist in a mixture of hematite (Fe_2O_3) and $FeOHSO_4$. When PD is performed using $(NH_4)_2Fe(SO_4)_2$, the $FeOHSO_4$ phase tends to disappear in favor of Fe_2O_3 and mikasaite ($Fe_2(SO_4)_3$), especially for the PD conducted at 100 °C. This transformation can be explained by the influence of heat, which promotes the conversion of $Fe(OH)SO_4$ into $Fe_2(SO_4)_3$, subsequently transforming into Fe_2O_3 (Eq. (7) [29,30]. Knowing this, it is worth noting that although the $Fe_2(SO_4)_3$ phase is not observed on the X-ray diffractograms of $FeSO_4$ + PD (3 h–100 °C) and + PD (72 h-25 °C) samples, it could still be formed through the transformation of $FeOHSO_4$ but in an amorphous state.

EDX and XPS data confirm the presence of iron sulfate phases in each solid, as indicated by the presence of sulfur and the position of the S2p peak around 169 eV (Supplementary information SI.2) [31]. Additionally, the data reveals the presence of nitrogen in the solids derived from $(NH_4)_2Fe(SO_4)_2$, suggesting the likely formation of another phase containing NH_4^+ (as indicated by the position of the N1s peak around 402 eV (Supplementary information SI.2)), which was not observed by XRD (Table 4) [31]. Moreover, the at % of each element at the surface and in bulk significantly differs, indicating the heterogeneous composition of the precipitates. Furthermore, the at % of S at the surface is higher than in the bulk, implying that iron sulfate phases predominantly exist on the outer layer of the solids (Table 4). Furthermore, since there is no significant variation in the binding energy of Fe and O elements, it can be concluded that the valence of these elements remains the same across varying synthesis conditions (Supplementary information SI.2).

For catalytic purposes, our primary interest lies in promoting the formation of more iron oxide and fewer iron sulfate phases since sulfur is known to act as a poison in reactions like total oxidation for depollution purposes [32]. An ideal solid for depollution catalysis should have a reduced S content and a Fe/O ratio increasing towards 0.67. A solid containing a higher proportion of Fe_2O_3 (Fe/O = 0.67) in comparison to

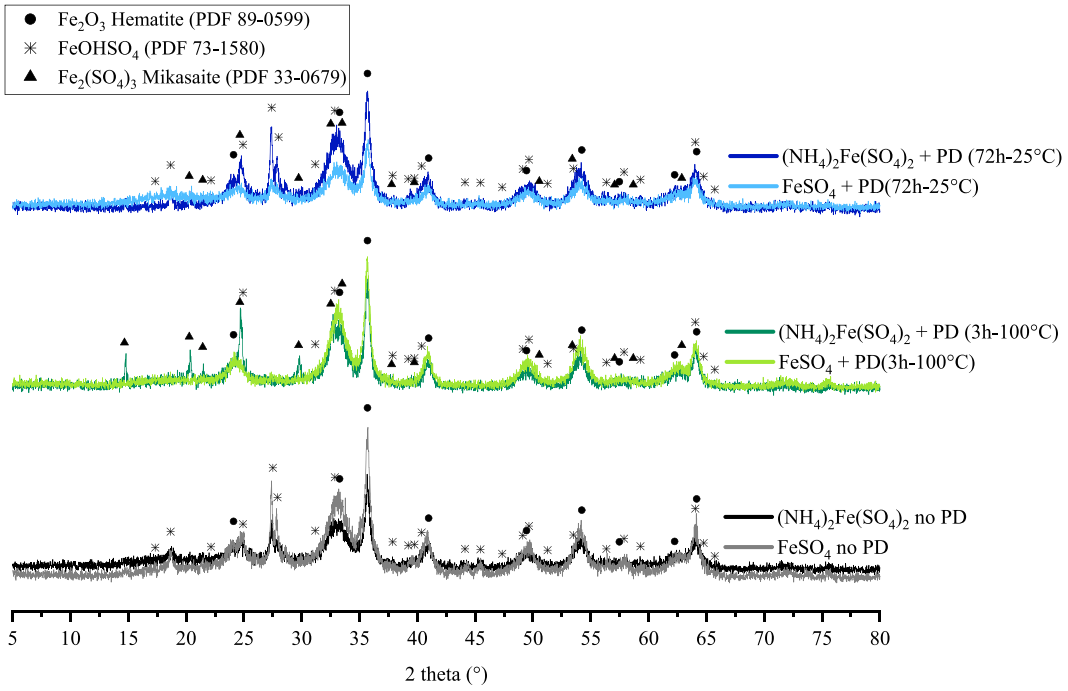

Fig. 2. XRD data of solids obtained with iron precursors without and with PD (3 h-100 °C and 72 h-25 °C).

Table 4
XPS and EDX data of solids obtained with iron precursors without and with PD (3 h-100 °C and 72 h-25 °C).

	Fe (at %)		O (at %)		S (% at)		N (% at)	Fe/O
	XPS (Fe2p)	EDX	XPS (O1s)	EDX *	XPS (S2p)	EDX	XPS (N1s)	XPS
$(NH_4)_2Fe(SO_4)_2$ no PD	23.9	26	66.5	72	6.5	2	3.1	0.36
$(NH_4)_2Fe(SO_4)_2$ + PD (3 h-100 °C)	27.7	30	65.6	67	5.3	2	1.3	0.42
$(NH_4)_2Fe(SO_4)_2$ + PD (72 h-25 °C)	28.1	31	65.8	67	4.9	3	1.2	0.42
$FeSO_4$ no PD	26.5	28	66.6	69	6.8	3	/	0.40
$FeSO_4$ + PD (3 h-100 °C)	30.2	22	65.7	77	4.1	1	/	0.46
$FeSO_4$ + PD (72 h-25 °C)	26.0	22	67.4	76	6.6	2	/	0.39

* The at % of O obtained by EDX is likely overestimated due to the underlying adhesive carbon tape used to fix the sample.

$FeOHSO_4$ (Fe/O = 0.2) and/or $Fe_2(SO_4)_3$ (Fe/O = 0.17) achieves a Fe/O ratio closer to 0.67. For both types of PD (3 h-100 °C and 72 h-25 °C), the at % of S decreases, and the Fe/O ratio at the surface increases toward 0.67 (Table 4). This shows that the development of Fe_2O_3 occurs at the expense of iron sulfate. The at % of S and Fe/O ratio after the PD at 25 °C for 72 h is close to those after the PD at 100 °C for 3 h, especially with $(NH_4)_2Fe(SO_4)_2$ (Table 4). This suggests that the application of heat during PD accelerates the transformation.

The provided information allows for imagining a reaction mechanism involving iron precursors during plasma discharge and during the subsequent PD steps. A. Tiya Djowe et al previously proposed a 2-step solid formation mechanism for $(NH_4)_2Fe(SO_4)_2$ involving OH° radicals [15]. However, our findings differ from their results, as we previously demonstrated that the primary plasma species driving the oxidoreduction leading to precipitation are instead the HNO_2/NO_2^- species [33]. Considering this, we proposed an alternative hypothetical mechanism. Given our understanding that, during the plasma discharge, a solid composed of FeOOH and $FeOHSO_4$ is formed, with the sulfate phase primarily located at the solid's surface, it is likely that a 3-step formation process of these 2 phases takes place [33]:

1) Firstly, it is probable that the Fe^{2+} ions originating from the precursor undergo oxidation by plasma species, resulting in the formation of Fe^{3+} (Eq. (3)):

$$Fe^{2+} + NO_2^- + 2H^+ \rightarrow Fe^{3+} + NO^\circ + H_2O \quad (3)$$

2) In an aqueous environment, Fe^{3+} ions are unstable, prompting their spontaneous hydrolysis into FeOOH if the medium is not sufficiently acidic (which subsequently transforms into Fe_2O_3 through calcination) [34] (Eq. (4)):

$$Fe^{3+} + 2H_2O \rightarrow FeOOH + 3H^+ \quad (4)$$

3) Additionally, Fe^{3+} can also react with other ions present in the medium, such as SO_4^{2-} ions originating from the precursor (Eq. (5)):

$$Fe^{3+} + SO_4^{2-} + H_2O \rightarrow FeOHSO_4 + H^+ \quad (5)$$

Given that the concentration of SO_4^{2-} is lower than that of H_2O, the likelihood of this last reaction taking place is lower. Consequently, a

reduced formation of the $FeOHSO_4$ phase occurs. Furthermore, since Fe^{3+} formed ions initially react with H_2O molecules, the availability of SO_4^{2-} ions probably increases with exposure time, which means that the likelihood of $FeOHSO_4$ formation increases with time, leading to its formation mostly at the surface of the already formed FeOOH. Imagining a formation process like this could provide a plausible explanation for the type of solid we observe, wherein a core primarily composed of FeOOH and a shell predominantly composed of FeOHSO4 are formed (Fig. 3).

During the PD step, various mechanisms can still occur. Firstly, HNO_2/NO_2^- has been identified as the primary species responsible for the oxidation of the precursors exposed to the glidarc plasma [33]. This species has a sufficiently long lifetime to remain present during the PD (Supplementary information SI.3) [14]. Consequently, Fe^{2+} from the precursor that was not oxidized during the discharge may have enough time to be transformed into Fe^{3+} by these HNO_2/NO_2^- species during the PD step. This could explain the increased amount of precipitate recovered when a PD step is performed (Table 3). Additionally, the Fe^{3+} ions formed both during the discharge and the PD step can still react with the remaining H_2O and SO_4^{2-} in the solution. Thereby, FeOOH and iron sulfate phases can further be created. This can occur either at the surface of previously formed particles or lead to the formation of new particles.

However, other phenomena can take place during this stage without being influenced by the plasma species generated. As suggested by the XPS results, this primarily occurs at the surface of particles already formed during the discharge. $FeOHSO_4$ can indeed react with water to form FeOOH, but it can also decompose into $Fe_2(SO_4)_3$ and FeOOH (Eq. (6); Eq. (7)). This can explain the increased amount of Fe_2O_3 present in the solid and at its surface, as well as the appearance of $Fe_2(SO_4)_3$. However, since the transformation of $FeOHSO_4$ is more efficient under heat, it can explain why solids formed from a PD performed at 100 °C have a reduced presence of this phase (Fig. 3) [29].

$$Fe(OH)SO_4 + H_2O \rightarrow FeOOH + H_2SO_4 \quad (6)$$

$$3FeOHSO_4 \rightarrow Fe_2(SO_4)_3 + FeOOH + H_2O \quad (7)$$

At this stage, it is understood that both types of PD facilitate the gradual transformation of the iron sulfate phase into iron oxide. Nevertheless, the supply of energy to the system seems to help accelerate this transformation (Fig. 3).

Regarding the change in solid morphology during the PD process, the growth of FeOOH crystals has previously been investigated by A. Tiya Dowe with $(NH_4)_2Fe(SO_4)_2$ as a precursor [35]. It was observed that during the PD, the particles agglomerate and develop into sea-urchin like hollow spheres, thereby enhancing their specific surface area and pore volume (Supplementary information SI.4, Fig. 3). In our study, comparable findings were noted for the solid formed using both iron precursors. When PD is performed at 100 °C for 3 h and at 25 °C for 72 h, solids develop cavities and form crystals with more spikes on their surface, thereby increasing the specific surface area of the solid (Supplementary information SI.5, Fig. 4). When performing the PD at 100 °C, alongside the emergence of spikes, we observe the formation of the "sea-urchin like" crystals for both precursors. This observation indicates that applying heat during the PD step facilitates the advancement of crystal development (Fig. 4 (b)). Consequently, conducting PD results in solids with a larger specific surface area and pore volume for both precursors, especially when done at 100 °C for 3 h (Table 5).

In terms of catalytic activity of the solids derived from iron precursors, it is slightly enhanced when a PD is performed at 100 °C for 3 h for both precursors. However, the PD (72 h-25 °C) is only beneficial for catalyst produced from $(NH_4)_2Fe(SO_4)_2$ (Fig. 5). These results align with previously identified characteristics. As the PD process increases the presence of the catalytically active phase (Fe_2O_3) in the solid and slightly augments its specific surface area and pore volume, it accordingly enhances the catalytic activity of the resulting material. In the case of solids formed from iron precursors, the application of heat promotes the gradual transformation of the iron sulfate phase into iron oxide and improves the formation of crystals with a higher specific surface area and pore volume. Consequently, conducting the PD at 100 °C for 3 h has a more significant impact on the catalytic activity of the solid obtained from both precursors.

3.1.2. Tin precursors

The first observation is that the presence of plasma-generated species is not necessary for the reaction and precipitation of tin precursors, as even without plasma, a solid is formed (Table 6). This phenomenon arises from the instability of Sn^{2+} ions in a not acidic enough aqueous solution, causing them to spontaneously react and form $Sn(OH)_4$ [34]. Additionally, $SnSO_4$ and $SnCl_2$ in water tend to undergo hydrolysis, transforming into $Sn_3O(OH)_2SO_4$ and Sn(OH)Cl respectively [34,36–39]. However, through plasma synthesis, the quantity of recovered precipitate significantly surpasses that obtained without plasma (Table 6). This heightened yield is likely attributed to the oxidizing species generated by plasma. These species accelerate the oxidation of Sn^{2+} to Sn^{4+} and potentially also convert the intermediates $Sn_3O(OH)_2SO_4$ and Sn(OH)Cl into $Sn(OH)_4$. Moreover, the increased amount of recovered solid for both types of PD (3 h-100 °C and 72 h-25 °C) for the $SnCl_2$ precursor shows that this step enables the species created during the plasma discharge to persist in their reactivity, facilitating further precipitation.

The precursor solution is already acidic before plasma exposure, owing to the spontaneous formation of $Sn(OH)_4$, $Sn_3O(OH)_2SO_4$ and Sn(OH)Cl, which release H^+ ions in the medium when $SnSO_4$ and $SnCl_2$ are dissolved in water [34,37,39]. The exposure to plasma further acidifies the solution by generating H^+. Throughout the PD, the pH level remains relatively stable because the solution is already at a very low pH, where the HNO_2/NO_2^- couple present in the medium (pKa = 3.3) acts as a buffer. (Table 6) [40].

The XRD diffractograms of the solids derived from tin precursors reveal that the phases developed before and after both PD (3 h-100 °C and 72 h-25 °C) remain unchanged. In both precursors, the phase developed is cassiterite (SnO_2), resulting from the dehydration of the $Sn(OH)_4$ formed in solution during the solid's drying steps (Supplementary information SI.7). However, the presence of S and Cl detected by XPS and EDX for solids obtained from $SnSO_4$ and $SnCl_2$ respectively, suggests the possible development of another amorphous phase (Table 7). These phases could be Sn(OH)Cl and $Sn_3O(OH)_2SO_4$, formed through the hydrolysis of $SnSO_4$ and $SnCl_2$ respectively, as previously explained [34,37,39]. This speculation gains support from the binding energy measured by XPS, as the Cl1s peak position around 199 eV corresponds to that of chlorine atoms linked with a transition metal, and the S1s peak position around 169 eV aligns with that of a sulfate element

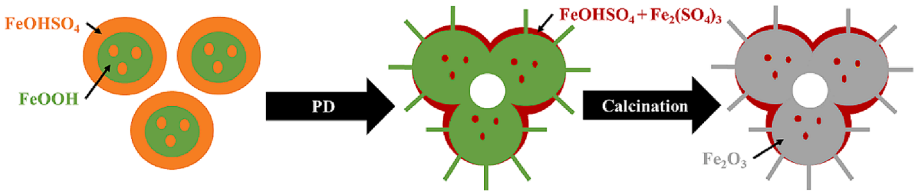

Fig. 3. Mechanism of formation of solids obtained with iron precursors without and with PD.

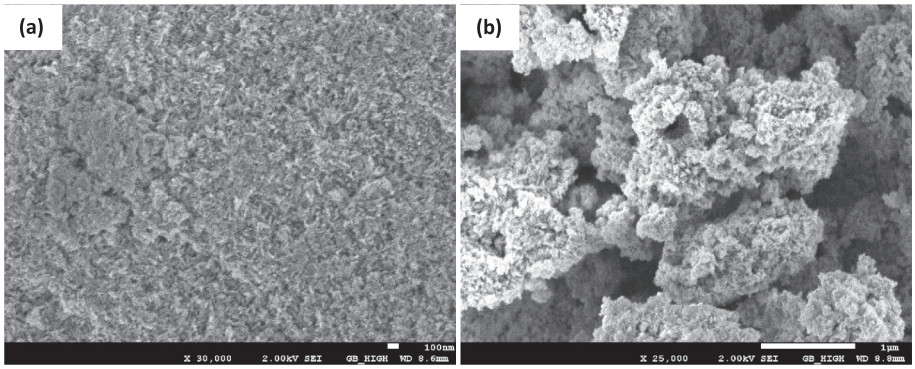

Fig. 4. SEM images of solids formed from $(NH_4)_2Fe(SO_4)_2$ (a) no PD; (b) + PD (3 h-100 °C).

Table 5
Textural properties obtained by N_2-physisorption with iron precursors without and with PD (3 h-100 °C and 72 h-25 °C) (isotherms Supplementary information SI.6).

	Specific surface area (m^2/g)	Pore volume (cm^3/g)
$(NH_4)_2Fe(SO_4)_2$ no PD	69	0.18
$(NH_4)_2Fe(SO_4)_2$ + PD (3 h-100 °C)	112	0.30
$(NH_4)_2Fe(SO_4)_2$ + PD (72 h-25 °C)	80	0.22
$FeSO_4$ no PD	95	0.33
$FeSO_4$ + PD (3 h-100 °C)	133	0.34
$FeSO_4$ + PD (72 h-25 °C)	63	0.17

(Supplementary information SI.8) [23,39]. Concerning the binding energy of the other elements (Sn and O), no significant variation is observed. Therefore, it can be concluded that the valence of these elements remains the same across varying synthesis conditions (Supplementary information SI.8).

XPS and EDX data highlight that the at % of each element at the surface and in bulk significantly differs, indicating the heterogeneous composition of the precipitates. Furthermore, the at % of S and Cl at the surface is higher than in bulk, implying that iron sulfate or iron chloride phases predominantly exist on the outer layer of the solids (Table 7).

For catalytic purposes, our primary interest lies in promoting the formation of more tin oxide and less tin sulfate or tin chloride phases since sulfur and chloride are known to act as poisons in reactions like total oxidation for depollution purposes [41–43]. Therefore, an ideal solid for depollution catalysis should have a reduced S and Cl content and a Sn/O ratio closer to 0.5. A solid containing a higher proportion of SnO_2 (Sn/O = 0.5) than $Sn_3O(OH)_2SO_4$ (Sn/O = 0.43) or Sn(OH)Cl (Sn/O = 1) achieves a Sn/O ratio closer to 0.5. For both types of PD, the at % of S and Cl decreases at the surface, but the PD performed at 25 °C for 72 h has the most effective impact. Consequently, the development of tin oxide occurs at the expense of tin sulfate or tin chloride, at the surface of the solid. In bulk, the at % of S and Cl is already close to 0, so no big change is observed (Table 7).

However, regarding the Sn/O ratio, even before the PD, the value exceeds 0.5 and becomes even larger afterward (Table 7). This scenario is not feasible if only SnO_2, as tin oxide, is formed during the transformation of tin sulfate or tin chloride. Our observations therefore imply

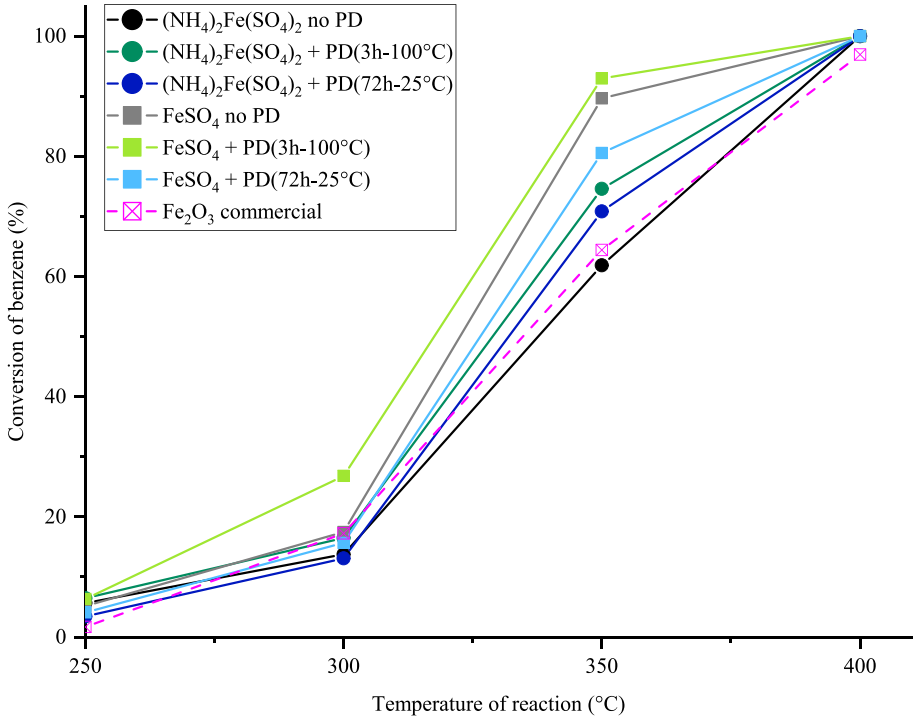

Fig. 5. Catalytic performances of solids formed from iron precursors without and with PD (3 h-100 °C and 72 h-25 °C) for the total oxidation of benzene (conversion of benzene as function of temperature reaction).

Table 6
Mass of solid produced and pH of the solution when tin precursors are exposed to the glidarc plasma without PD, with PD (3 h-100 °C and 72 h-25 °C) and without plasma.

	Mass of solid produced (g)		pH		
	After exposure/ PD	After no plasma exposure	Precursor solution	After exposure	After PD
$SnSO_4$ no PD	0.686	0.156	2.5	2	/
$SnSO_4$ + PD (3 h-100 °C)	0.681	0.356			1.9
$SnSO_4$ + PD (72 h-25 °C)	0.677	0.336			1.8
$SnCl_2$ no PD	0.674	0.069			/
$SnCl_2$ + PD (3 h-100 °C)	0.723	0.406			1.8
$SnCl_2$ + PD (72 h-25 °C)	0.705	0.023			1.7

Table 7
XPS and EDX data of solids obtained with tin precursors without and with PD (3 h-100 °C and 72 h-25 °C).

	Sn (at %)		O (at %)		S or Cl (at %)		Sn/ O
	XPS (Sn3d)	EDX	XPS (O1s)	EDX *	XPS (S2p or Cl1s)	EDX	XPS
$SnSO_4$ no PD	33.5	14	63.5	85	2.9	1	0.53
$SnSO_4$ + PD (3 h-100 °C)	35.2	17	62.4	81	2.5	1	0.56
$SnSO_4$ + PD (72 h-25 °C)	36.5	21	61.3	79	2.2	1	0.58
$SnCl_2$ no PD	35.2	29	63.4	71	1.4	0	0.56
$SnCl_2$ + PD (3 h-100 °C)	36.7	25	62.4	75	0.9	0	0.59
$SnCl_2$ + PD (72 h-25 °C)	38.7	25	60.7	74	0.5	0	0.64

* The at % of O obtained by EDX is likely overestimated due to the underlying adhesive carbon tape used to fix the sample.

the presence of another unidentified phase with a Sn/O ratio > 0.5 in the solid. This could be SnO (Sn/O = 1) from $Sn_3O(OH)_2SO_4$ or Sn(OH)Cl that has not had the opportunity to oxidize and subsequently transforms into tin(II) oxide. This might explain the observed increased Sn/O ratio after PD.

With the above information, we propose a hypothetical reaction mechanism for $SnSO_4$ and $SnCl_2$ exposed to plasma discharge as follows:

1) Firstly, either Sn^{2+} ions resulting from the dissolution of $SnSO_4$ and $SnCl_2$ precursors spontaneously oxidize to form $Sn(OH)_4$ (Eq. (8)), or the precursors undergo hydrolysis in water to produce tin hydroxy sulfate or tin hydroxy chloride (Eq. (9); Eq. (10)). In fact, in solution with Cl^- or SO_4^{2-} ions at pH = 2.5, Sn^{2+} does not form the tin hydroxide $Sn(OH)_2$ but instead prefers to transform into these components, which are more stable [34,36–39]:

$$Sn^{2+} + 4H_2O \rightarrow Sn(OH)_4 + 4H^+ + 2e^- \quad (8)$$

$$3SnSO_4 + 3H_2O \rightarrow Sn_3O(OH)_2SO_4 + 4H^+ + 2SO_4^{2-} \quad (9)$$

$$SnCl_2 + H_2O \rightarrow Sn(OH)Cl + HCl \quad (10)$$

2) Subsequently, Sn^{2+} ions that have not had sufficient time to react spontaneously with water and tin sulfate or tin chloride intermediates formed previously can be oxidized by the plasma species into $Sn(OH)_4$ [33] (Eq. (11)):

$$Sn^{2+} + 2NO_2^- \rightarrow Sn(OH)_4 + 2NO^\circ + H_2O \quad (11)$$

In the process of transforming $Sn_3O(OH)_2SO_4$ or Sn(OH)Cl particles into $Sn(OH)_4$, it is conceivable that upon their transformation, these particles undergo rapid oxidation by plasma species, preventing them from being "trapped" within the particle core. Consequently, when plasma exposure ceases, the unoxidized portion of the precipitate predominantly resides on the solid's surface. This phenomenon could explain the absence of S or Cl in the material's bulk (Fig. 6).

Afterward, as $Sn(OH)_4$ is less stable than Sn(IV) oxide, the application of heat during the drying steps leads to the spontaneous dehydration of $Sn(OH)_4$, resulting in SnO_2, which is the phase observed by XRD (Eq. (12); Supplementary information SI.7, Fig. 6).

$$Sn(OH)_4 \rightarrow SnO_2 + 2H_2O \quad (12)$$

Throughout the PD step, NO_2^- is still present due to its extended lifespan, allowing it to probably continue oxidizing some $Sn_3O(OH)_2SO_4$ or Sn(OH)Cl particles into $Sn(OH)_4$. However, NO_2^-, which is no longer generated during this step, tends to transform into NO_3^-, thus hindering its ability to completely oxidize these phases (Supplementary information SI.3) [34]. Consequently, some $Sn_3O(OH)_2SO_4$ or Sn(OH)Cl may simply decompose into $Sn(OH)_2$, which is later transformed to SnO during the drying step (Eq. (13), Eq. (14), Eq. (15); Fig. 6). This hypothesis fits with the observed increased Sn/O ratio during the PD step. Furthermore, even though the PD at 25 °C for 72 h has a more significant impact on transforming sulfate and chloride phases, the PD performed at 100 °C for 3 h already effectively transforms these phases. It appears that applying heat to the system seems to accelerate the transformation, which would probably occur anyway under ambient temperature conditions if given sufficient time.

$$Sn_3O(OH)_2SO_4 + 3H_2O \rightarrow 3Sn(OH)_2 + SO_4^{2-} + 2H^+ \quad (13)$$

$$Sn(OH)Cl + H_2O \rightarrow Sn(OH)_2 + Cl^- + H^+ \quad (14)$$

$$Sn(OH)_2 \rightarrow SnO + H_2O \quad (15)$$

Regarding the change in solid morphology during the PD process, for both precursors, the specific surface area of the solid decreases without changing the pore volume (Table 8). This is likely a result of particle agglomeration due to heat and time.

Regarding the catalytic activity of solids derived from tin precursors, it is enhanced when a PD is performed at 100 °C and 25 °C for both, but the 72 h PD demonstrates a superior effect, especially for $SnSO_4$ (Fig. 7). These results align with previously identified characteristics. As the PD process leads to an increased presence of the catalytically active phase (tin (IV and II) oxide) at the surface of the solid, particularly when conducted at 25 °C, it thereby enhances its catalytic activity. However, in both cases, the specific surface area of the solids diminishes when a PD step is performed, especially when done at 25 °C for 72 h. This implies that augmenting the quantity of the catalytically active phase has a more significant impact than the decrease in specific surface area. Consequently, conducting the PD at 25 °C has a more significant impact on the catalytic activity of the solid in both cases.

3.1.3. What are the similar impacts of the PD on precursors exposed to the GP?

At this stage, we cannot assert that a particular type of PD consistently yields superior results by developing more interesting characteristics for all types of plasma-synthesized solids. However, when considering the influence of the PD step on precursor salts of the same

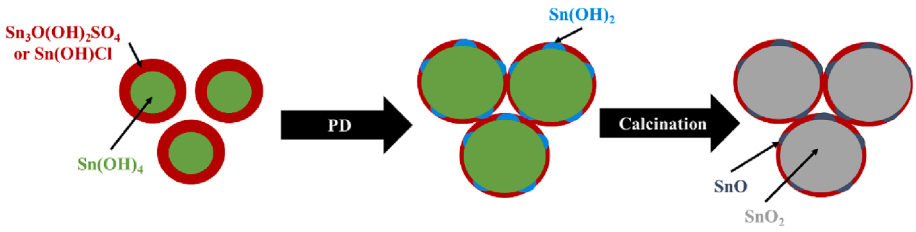

Fig. 6. Mechanism of formation of solids obtained with tin precursors without and with PD.

Table 8
Textural properties obtained by N2-physisorption with tin precursors without and with PD (isotherms Supplementary information SI.9).

	Specific surface area (m^2/g)	Pore volume (cm^3/g)
$SnSO_4$ no PD	162	0.13
$SnSO_4$ + PD (3 h-100 °C)	140	0.15
$SnSO_4$ + PD (72 h-25 °C)	132	0.14
$SnCl_2$ no PD	146	0.11
$SnCl_2$ + PD (3 h-100 °C)	110	0.11
$SnCl_2$ + PD (72 h-25 °C)	89	0.11

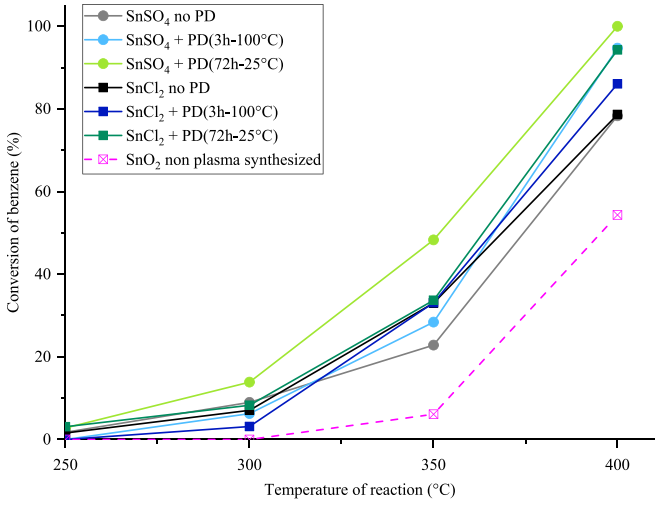

Fig. 7. Catalytic performances of solids formed from tin precursors without and with PD for the total oxidation of benzene (conversion of benzene as function of temperature reaction).

metal, a discernible pattern emerges. Specifically, solids obtained from different precursors of the same metal exhibit identically superior catalytic activity when synthesized under similar conditions. Precisely, in the case of iron precursors, the PD at 100 °C yields the most interesting properties, while for tin precursors, the PD at 25 °C proves most promising. This suggests that we may be able to anticipate in advance the preferable type of PD to conduct when using a new precursor of a metal previously studied with a different precursor.

Although the impact of each PD type varies for different metal precursors, a global effect can still be observed. Firstly, the PDs do not fundamentally alter the type of solid formed. Instead, a phase formed during the plasma discharge is more or less present after the PD due to the transformation from one phase to another. Consequently, the same atoms remain in the solid after the PD, but not in the same atomic percentage. Additionally, all tested precursors tend to form a sulfate or chlorate phase, primarily located at the solid surface during the plasma discharge. Throughout each PD type, this intermediate appears to transform into a metal oxide. Furthermore, the PD invariably influences the textural properties of the solid. While the pore volume may not always change, the specific surface area does. Due to factors like time and temperature, particles formed during plasma discharge tend to agglomerate. However, this does not consistently result in a decrease in a specific surface area. Depending on crystal growth patterns, some roughness and porosity can be created, thereby increasing the solid's specific surface area. Certainly, the fact that PD affects various solid characteristics leads to changes in its catalytic activity. The activity improves when the catalytically active phase increases and/or the specific area increases, but it worsens if the opposite occurs.

However, in nearly all cases, conducting a PD at either 100 °C or 25 °C enhances catalytic performance, with the exception of $FeSO_4$ + PD (72 h-25 °C). This suggests that incorporating a PD step is almost always beneficial. If a quicker synthesis is preferred, the PD at 100 °C is the more compelling choice. Alternatively, if a synthesis method requiring less energy input and resulting in a higher yield of recovered solids is desired, the PD at 25 °C is more suitable. These results indicate that, depending on the synthesis parameters of preference, one PD may outperform another, but the addition of a PD step consistently proves to be a constructive way to enhance the performance of a plasma-synthesized catalyst.

Furthermore, it has been observed that the amount of solid recovered is impacted when a PD is performed. For most precursors, allowing more time for the solid to develop increases the quantity of recovered solid. Hence, although there are instances where the catalytic performance of the catalysts does not exhibit a significant change, questioning the necessity of adding a PD step, it consistently enhances the yield of solid formation. Therefore, incorporating a PD step is an effective way to enhance the overall plasma synthesis for two reasons: by augmenting the yield of solid formation while increasing its catalytic activity.

3.2. *Elucidation of the mechanism underlying the PD*

We have demonstrated that PD is an interesting step to apply in the GP synthesis, enhancing the yield of recovered solids and enabling the development of catalysts with more interesting properties. However, the exact mechanism behind this step remains unclear. Some hypotheses proposed in the literature suggest that the species generated during the PD (H_2O_2, HNO_3, HNO_2, etc) influence the modification of the solid. Actually, these hypotheses were never proven before. Therefore, our objective is to comprehend the functioning of the PD step and determine whether the plasma species present during the PD indeed impact the modification of GP-synthesized solids. To address this, we compared solids obtained from $(NH_4)_2Fe(SO_4)_2$ and $SnSO_4$ subjected to a classical PD step with solids developed when a PD is conducted without the presence of plasma species.

The diffractograms obtained for these solids reveal that the phases developed when the PD is performed with or without the presence of plasma species are identical for $(NH_4)_2Fe(SO_4)_2$ and $SnSO_4$ in both types of PD (Fig. 8, Supplementary information SI.10).

By comparing the at % of elements present in solids synthesized with and without plasma species during the PD step, it is evident that they rarely exhibit really close similarities (Table 4, Table 7, Table 9). Notably, the only samples demonstrating a relatively similar elemental composition are the solids formed from $(NH_4)_2Fe(SO_4)_2$ with a PD(3 h–100 °C). However, certain commonalities are observable. Firstly, the

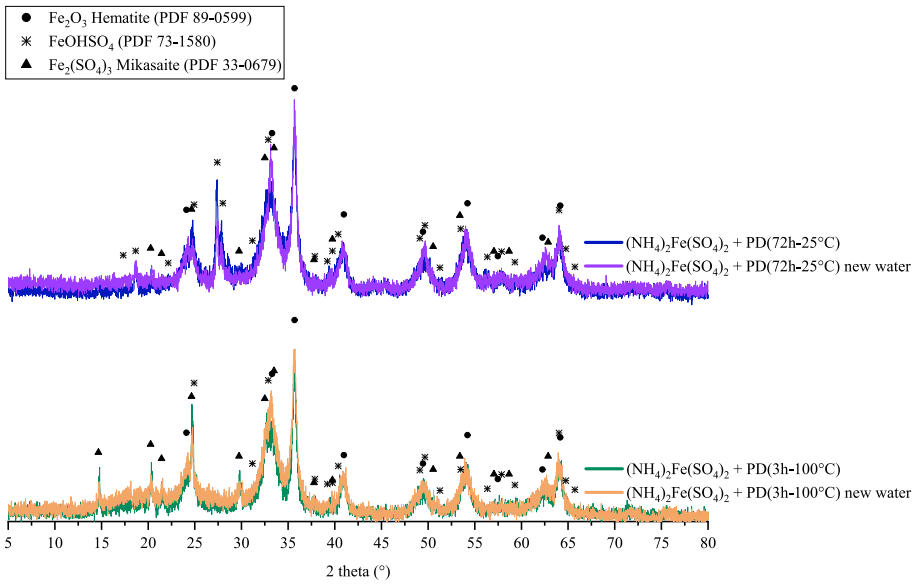

Fig. 8. XRD data of solids obtained with $(NH_4)_2Fe(SO_4)_2$ with PD with and without plasma species.

binding energy of S2p around 169 eV as determined by XPS, constantly corresponds to SO_4^{2-}, as previously observed (Supplementary information SI.11). Furthermore, the changes occurring within the solid during the PD step remain consistent, regardless of the presence of plasma species. Specifically, the at % of S decreases, while the at % of Sn or Fe increases (Table 4, Table 7, Table 9). This suggests that the plasma-generated species present during the PD are not essential for triggering the observed transformation that typically occurs during this step, which is the conversion of iron or tin sulfates into iron or tin oxides.

The at % of S is smaller, while the at % of Fe or Sn is higher in almost all cases when the PD is done without plasma species (Table 4, Table 7, Table 9). This can be attributed to the "washing step" conducted by recovering the synthesized solid after the discharge and immersing it in fresh distilled water. This step not only removes the plasma-generated species but also eliminates other ions, including SO_4^{2-}. Consequently, these species can no longer interact with the synthesized solid and, therefore, cannot be deposited on its surface, diminishing the formation of the sulfates during this step.

Regarding their texture, it is evident that the changes in the solid are consistent, regardless of the presence of plasma species during the PD step (Table 5, Table 8, Table 10). When the PD is performed at 100 °C for $(NH_4)_2Fe(SO_4)_2$, the specific surface area and pore volume increase. However, these features decrease when the PD is carried out at 25 °C for the $(NH_4)_2Fe(SO_4)_2$ and for both PD involving $SnSO_4$.

Finally, regarding their catalytic activity, both precursors, irrespective of plasma species presence during PD, yield solids with higher catalytic activity (Fig. 9). This is attributed to the consistency in solid transformation, whether plasma species are present or not. In fact, although the catalytic activities of solids synthesized with or without plasma species present in the PD may not be identical, we have observed a consistent pattern of solid transformation that tends to enhance catalytic activity. Therefore, these modifications result in a similar impact on the catalytic test, regardless of the presence of plasma species during the PD, ultimately improving it compared to when no PD is performed.

With the above information, in contrast to earlier suggestions in the literature, we can conclude that species generated by plasma do not play a role in the solid transformations occurring during the PD step. The phases conversion and crystal growth observed in this process primarily reflect a maturation step that involves the solid in a specific manner, contingent upon the applied heat and the duration of the step.

In classical plasma applications, the term "post-discharge" holds a different meaning than in glidarc plasma. It is defined as "the area downstream of the discharge, where the species produced by the discharge are entrained by a gaseous or liquid flow but are no longer influenced by the electric field" [44]. In the gold nanoparticles (NPs) synthesis described by Mariotti et al., it is explained that within the

Table 9
XPS and EDX data of solids obtained with $(NH_4)_2Fe(SO_4)_2$ and $SnSO_4$ with PD without plasma species.

	Fe or Sn (at%)		O (at%)		S (%at)		Fe/O or Sn/O
	XPS (Fe2p or Sn3d)	EDX	XPS (O1s)	EDX *	XPS (S2p)	EDX	XPS
$(NH_4)_2Fe(SO_4)_2$ + PD (3 h-100 °C) new water	28.1	31	65.6	66	5.2	3	0.43
$(NH_4)_2Fe(SO_4)_2$ + PD (72 h-25 °C) new water	31.6	31	64.7	67	3	3	0.49
$SnSO_4$ + PD (3 h-100 °C) new water	35.8	21	63.3	79	1	0	0.57
$SnSO_4$ + PD (72 h-25 °C) new water	34.9	20	62.9	80	2.3	1	0.55

* The at % of O obtained by EDX is likely overestimated due to the underlying adhesive carbon tape used to fix the sample.

Table 10
Textural properties obtained by N_2-physisorption of solids obtained with (a) $(NH_4)_2Fe(SO_4)_2$ and (b) $SnSO_4$ with PD with and without plasma species.

	Specific surface area (m^2/g)	Pore volume (cm^3/g)
$(NH_4)_2Fe(SO_4)_2$ + PD (3 h-100 °C) new water	105	0.30
$(NH_4)_2Fe(SO_4)_2$ + PD (72 h-25 °C) new water	74	0.28
$SnSO_4$ + PD (3 h-100 °C) new water	107	0.14
$SnSO_4$ + PD (72 h-25 °C) new water	120	0.14

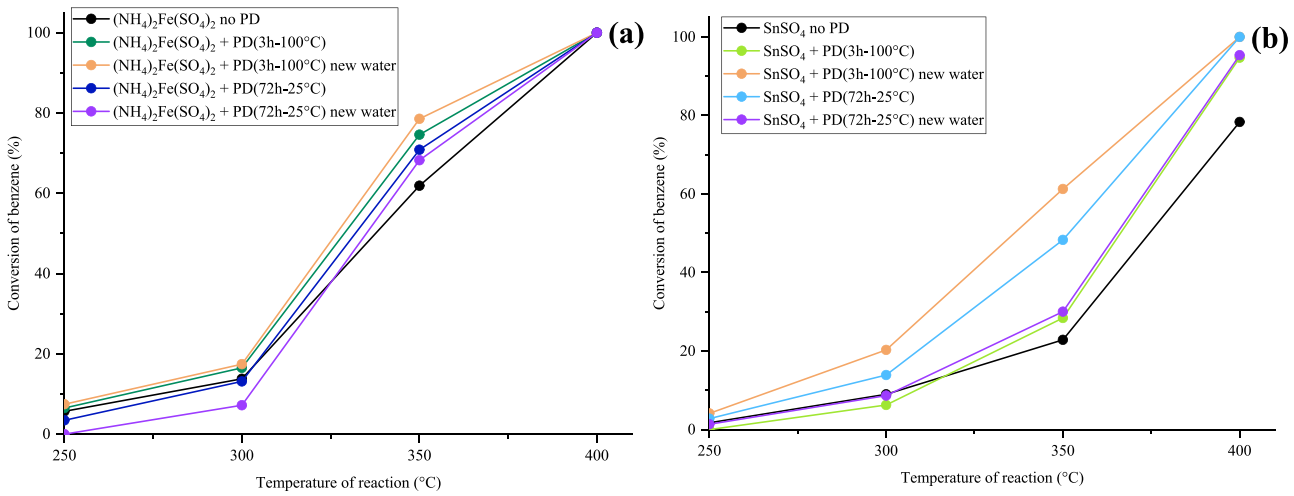

Fig. 9. Catalytic performances of solids formed with (a) $(NH_4)_2Fe(SO_4)_2$ and (b) $SnSO_4$ with PD with and without plasma species.

"plasma zone", where reactive species formed by the plasma discharge are concentrated, the precursor undergoes transformation into gold NPs, constituting the "nucleation step". Subsequently, when these particles exit this zone, they enter the "post-discharge zone" where the solid grows, leading to the development of larger particles (Fig. 10) [45]. Knowing this, we can draw a parallel between the PD step of glidarc plasma and classical plasma PD. In both cases, when the precursor is exposed to the plasma discharge, it interacts with the plasma species to form a precipitate. Subsequently, when the solid is placed in PD, it undergoes a "maturation step", influenced by the duration and temperature of the PD process.

Nevertheless, although it can be concluded that plasma species do not contribute to the transformation during the PD of already precipitated solids, it can be asserted that they do influence the reaction of metal ions from the precursor that have not had sufficient time to react during the discharge. This is evidenced by the increased amount of recovered precipitate when iron and tin precursors undergo the PD step (Table 3, Table 6). In fact, we have previously established that NO_2^- is the main species responsible for the precipitation process and that it persists long enough to be present during the PD step (Supplementary information SI.3) [14,33]. Therefore, these species do still initiate the transformation of metal ion precursors remaining in solution. However, once the discharge is shut down, no more NO_2^- species are generated, and they tend to decompose into NO_3^- (which has been identified as not triggering the reaction) (Supplementary information SI.3) [33,34]. Consequently, they cannot remain present in sufficient amounts to facilitate the reaction of all the remaining metal ion precursors in solution.

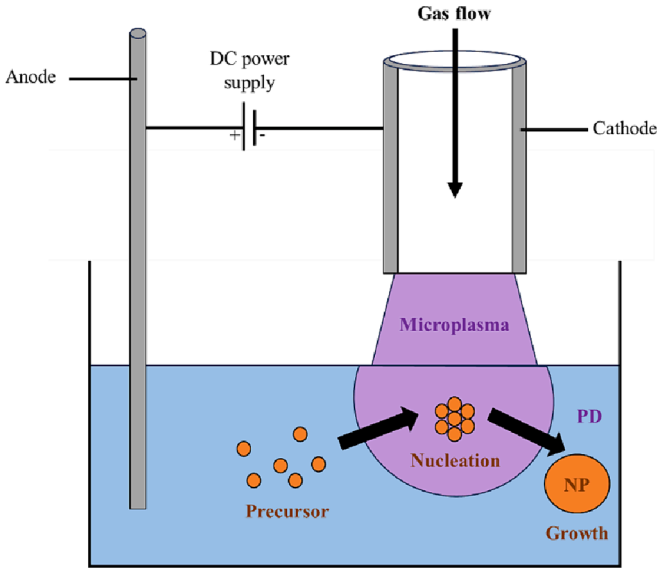

Fig. 10. Schematic diagrams depicting the microplasma set-up used for NPs synthesis.
adapted from [45]

4. Conclusion

GP catalyst synthesis offers interesting conditions when compared to alternative synthesis methods, such as mild conditions and short processing time. Additionally, this approach can be considered eco-friendly and cost-effective, as the only chemical used to generate these reactive species is water-saturated air, which is non-polluting, available, and renewable. Nonetheless, while catalysts synthesized through this method already exhibit promising characteristics and catalytic activity, enhancing the method by introducing a new synthesis step while preserving its advantageous parameters presents an opportunity to further improve its interest.

As previously suggested in the literature for FeO_x and MnO_x derived from $(NH_4)_2Fe(SO_4)_2$ and $KMnO_4$ synthesized through GP exposure, we confirm that the PD step is valuable to all types of solids synthesized from various precursors. Regardless of the precursor type, conducting a PD either at 100 °C or 25 °C proves to be an interesting process to increase the quantity of recovered solids and/or bring interesting new characteristics to the catalyst. Moreover, we observed similar transformations occurring during the PD, whatever the nature of the precursor salts used for a given metal. Specifically, solids with superior catalytic activity are consistently synthesized under comparable conditions for each metal. In our study, solids synthesized from iron precursors exhibit enhanced catalytic activity when the PD is performed at 100 °C, whereas for tin precursors, the PD at 25 °C shows the most promising results.

Although the impact of each PD type varies from precursors to one metal to another, a global effect is still apparent. That is the transformation of sulfate or chloride phases into metal oxides, the influence on the solid's textural properties, the increase in the amount of recovered solid, and the corresponding modification of its catalytic activity.

However, in nearly all cases, conducting a PD at either 100 °C or 25 °C enhances the catalytic performance of GP-synthesized solids. This means that, depending on the synthesis parameters of preference, such as a lower synthesis time, less energy input, or a higher yield of recovered solid, one PD may outperform another.

Consequently, the PD step has proven to be a crucial stage to implement in plasma-synthesized catalysts. However, contrary to what was stated before, our experiments show that species generated by plasma do not play a role in the solid transformations occurring during the PD step. In fact, we demonstrate that, whether plasma species are present during the PD step or not, the transformations occurring in the solid remain consistent. The phases conversion and crystal growth observed in this process primarily reflect a maturation step that involves the solid in a specific manner, contingent upon the applied heat and the duration of the step.

However, this does not imply that plasma species present during the PD step are irrelevant to the process. On the contrary, the NO_2^- remaining in solution during this stage does still facilitate the reaction of ion precursors remaining in solution when the discharge is switched off, transforming them into precipitates and thereby increasing the amount of solid formed.

CRediT authorship contribution statement

F. Hanon: Writing – original draft. **E.M. Gaigneaux:** Writing – review & editing, Supervision.

Declaration of competing interest

The authors declare the following financial interests/personal relationships which may be considered as potential competing interests: Hanon fanny reports financial support was provided by Fund for Scientific Research. Hanon Fanny reports a relationship with Fund for Scientific Research that includes: funding grants. If there are other authors, they declare that they have no known competing financial interests or personal relationships that could have appeared to influence the work reported in this paper.

Data availability

No data was used for the research described in the article.

Acknowledgments

Fanny Hanon acknowledges the FNRS for the FRIA scholarship no.40004581.

The authors gratefully acknowledge François Devred for the technical and logistical support, Michel Devillers and Sophie Hermans for the chemistry private lessons and advices, Pierre Eloy for access to the XPS instrument and Delphine Magnin for access to the SEM-EDX instrument.

Appendix A. Supplementary data

Supplementary data to this article can be found online at https://doi.org/10.1016/j.cej.2024.151088.

References

[1] J.M. Thomas, W.J. Thomas, Principles and practice of heterogeneous catalysis, VCH, Weinheim, 1997.
[2] D. Kolb, Catalysis, J. Chem. Educ. 56 (1979) 743–747.
[3] J. Védrine, Heterogeneous catalysis on metal oxides, Catalysts 7 (2017) 341.
[4] L. Lerner, 7 things you may not know about catalysis, Argonne Natl, Lab, 2011 https://www.anl.gov/article/7-things-you-may-not-know-about-catalysis (accessed April 15, 2020.
[5] J.W. Niemantsverdriet, Spectroscopy in catalysis: an introduction, 2nd ed., Wiley-VCH, Weinheim, 2000.
[6] J.F. Lepage, Catalyse de contact: conception, préparation et mise en oeuvre des catalyseurs industriels, Technip, Paris, 1978.
[7] A. Czernichowski, Gliding arc: applications to engineering and environment control, Pure Appl. Chem. 66 (1994).
[8] H. Lesueur, A. Czernichowsky, J. Chapelle, Dispositif de génération de plasma basse température par formation de décharges électriques glissantes, 2639172, n.d.
[9] M.R. Ghezzar, F. Abdelmalek, M. Belhadj, N. Benderdouche, A. Addou, Gliding arc plasma assisted photocatalytic degradation of anthraquinonic acid green 25 in solution with TiO2, Appl. Catal. B Environ. 72 (2007) 304–313.
[10] E.B. Tsagou-Sobze, D. Moussa, A. Doubla, E. Hnatiuc, J.-L. Brisset, Gliding discharge-induced oxidation of a toxic alkaloid, J. Hazard. Mater. 152 (2008) 446–449.
[11] A. Czernichowski, H. Nassar, A. Ranaivosoloarimanana, A.A. Fridman, M. Simek, K. Musiol, E. Pawelec, L. Dittrichova, Spectral and electrical diagnostics of gliding arc, Acta Phys. Pol. A 89 (1996) 595–603.
[12] A. Doubla, L. Boubabello, M. Fotso, J. Brisset, Plasmachemical decolourisation of Bromothymol Blue by gliding electric discharge at atmospheric pressure, Dyes Pigments 77 (2008) 118–124.
[13] A. El-Zein, M. Talaat, G. El-Aragi, A. El-Amawy, Electrical characteristics of nonthermal gliding arc discharge reactor in argon and nitrogen gases, IEEE Trans. Plasma Sci. 44 (2016) 1155–1159.
[14] J.-L. Brisset, D. Moussa, A. Doubla, E. Hnatiuc, B. Hnatiuc, G. Kamgang Youbi, J.-M. Herry, M. Naïtali, M.-N. Bellon-Fontaine, Chemical reactivity of discharges and temporal post-discharges in plasma treatment of aqueous media: examples of gliding discharge treated solutions, Ind. Eng. Chem. Res. 47 (2008) 5761–5781.
[15] A. Tiya-Djowe, S. Laminsi, G.L. Noupeyi, E.M. Gaigneaux, Non-thermal plasma synthesis of sea-urchin like α-FeOOH for the catalytic oxidation of Orange II in aqueous solution, Appl. Catal. B Environ. 176–177 (2015) 99–106.
[16] F.W.B. Tatchemo, S. Nzali, G. Kamgang Youbi, A. Tiya Djowe, D.K. Saa, E. Acayanka, S. Laminsi, E.M. Gaigneaux, Gliding arc plasma synthesis of MnO2 nanorods for the plasma-catalytic bleaching of azoïc amaranth red dye, Top. Catal. 60 (2017) 962–972.
[17] A. Tiya-Djowe, E. Acayanka, A.P. Mbouopda, W. Boyom-Tatchemo, S. Laminsi, E. M. Gaigneaux, Producing oxide catalysts by exploiting the chemistry of gliding arc atmospheric plasma in humid air, Catal. Today 334 (2019) 104–112.
[18] J.-L. Brisset, J. Pawlat, Chemical effects of air plasma species on aqueous solutes in direct and delayed exposure modes: discharge, post-discharge and plasma activated water, Plasma Chem. Plasma Process. 36 (2016) 355–381.
[19] B. Benstaali, P. Boubert, B.G. Cheron, A. Addou, J.L. Brisset, Density and rotational temperature measurements of the OH° and NO° radicals produced by a gliding arc in humid air, Plasma Chem. Plasma Process. 22 (2002) 553–571.
[20] D. Moussa, H. Vitrac, B.G. Chéron, E. Hnatiuc, A. Addou, J.L. Brisset, Acidity control of the oxidation reactions induced by non-thermal plasma treatment of aqueous effluents in pollutant abatment processes, Eur. Phys. J. Appl. Phys. 29 (2005) 308–312.
[21] E. Acayanka, D.S. Kuete, G.Y. Kamgang, S. Nzali, S. Laminsi, P.T. Ndifon, Synthesis, characterization and photocatalytic application of TiO2/SnO2 nanocomposite obtained under non-thermal plasma condition at atmospheric pressure, Plasma Chem. Plasma Process. 36 (2016) 799–811.
[22] A.P. Mbouopda, E. Acayanka, F.W. Boyom-Tatchemo, G.Y. Kamgang, A.M. Nzeufa, S. Laminsi, D. Richard, New-route synthesis of N-doped TiO2 via exposing the TiCl3 precursor to non-thermal quenched plasma at various times, Mater. Chem. Phys. 206 (2018) 224–231.
[23] A. Tiya-Djowe, M.-A. Dourges, H. Deleuze, Tuning the "O" vacancies density in SnO2 nanocrystals during and after humid air plasma synthesis: implications on the photocatalytic performances under UV light, J. Mater. Sci. 55 (2020) 4792–4807.
[24] F.W. Boyom-Tatchemo, F. Devred, G. Ndiffo-Yemeli, S. Laminsi, E.M. Gaigneaux, Plasma-induced redox reactions synthesis of nanosized α-, γ- and δ-MnO2 catalysts for dye degradation, Appl. Catal. B Environ. 260 (2020) 118159.
[25] E. Acayanka, A. Tiya Djowe, S. Laminsi, C.C. Tchoumkwé, S. Nzali, A. Poupi Mbouopda, P.T. Ndifon, E.M. Gaigneaux, Plasma-Assisted Synthesis of TiO2 Nanorods by Gliding Arc Discharge Processing at Atmospheric Pressure for Photocatalytic Applications, Plasma Chem. Plasma Process. 33 (2013) 725–735.
[26] A. Tiya-Djowe, N. Ruth, G. Kamgang-Youbi, E. Acayanka, S. Laminsi, E. M. Gaigneaux, FeOx-kaolinite catalysts prepared via a plasma-assisted hydrolytic precipitation approach for Fenton-like reaction, Microporous Mesoporous Mater. 255 (2018) 148–155.
[27] F.W. Boyom-Tatchemo, F. Devred, S. Laminsi, E.M. Gaigneaux, Temporal post-discharge reactions effect on the oxidative catalytic properties of plasma-synthesized α-MnO2 nanorods, Appl. Catal. Gen. 616 (2021) 118109.
[28] The International Centre for Diffraction Data, 2020. http://www.icdd.com/ (accessed March 27, 2020).
[29] P.K. Gallagher, D.W. Johnson, F. Schrey, Thermal Decomposition of Iron(II) Sulfates, J. Am. Ceram. Soc. 53 (1970) 666–670.
[30] G. Ventruti, G. Della Ventura, M.A. Gomez, G. Capitani, M. Sbroscia, A. Sodo, High-temperature study of basic ferric sulfate, FeOHSO4, Phys. Chem. Miner. 47 (2020) 43.
[31] X-ray Photoelectron Spectroscopy (XPS) Reference Pages, (n.d.). http://www.xpsfitting.com/search/label/Sulphur (accessed July 15, 2022).
[32] H.J. McAulay, G. Podolsky, F. Chan, Low sulfur red iron oxide useful as a catalyst or catalyst component and a process for making low sulfur red iron oxide, US 2007/0014716 A1, 2007.
[33] F. Hanon, S. Hermans, E.M. Gaigneaux, What are the species involved in the gliding arc plasma synthesis of heterogeneous catalysts? Catal. Today 430 (2024) 114550 https://doi.org/10.1016/j.cattod.2024.114550.
[34] M. Pourbaix, Atlas of electrochemical equilibria in aqueous solutions, National association of corrosion engineers, Cebelcor, Texas, Bruxelles, 1967.
[35] A. Tiya Djowe, Adsorbants et catalyseurs à base d'argile préparés par voie plasmachimique pour la dépollution des eaux résiduaires industrielles, Thèse, Université catholique de Louvain, Université De Yaoundé I (2014).

[36] C. House, G. Kelsall, Potential-pH diagrams for the Sn/H2O-Cl system, Electrochem. Acta 29 (1984) 1459–1464.
[37] R. Edwards, The stabilities of secondary tin minerals. Part 2*: The hydrolysis of tin (II) sulphate and the stability of Sn30(OH)2SO 4, (n.d.) 6.
[38] E. Kaprara, N. Tziarou, K. Kalaitzidou, K. Simeonidis, L. Balcells, E.V. Pannunzio, A. Zouboulis, M. Mitrakas, The use of Sn(II) oxy-hydroxides for the effective removal of Cr(VI) from water: Optimization of synthesis parameters, Sci. Total Environ. 605–606 (2017) 190–198, https://doi.org/10.1016/j.scitotenv.2017.06.199.
[39] G.G. Graf, Tin, Tin Alloys, and Tin Compounds, in: Wiley-VCH Verlag GmbH & Co. KGaA (Ed.), Ullmanns Encycl. Ind. Chem., Wiley-VCH Verlag GmbH & Co. KGaA, Weinheim, Germany, 2000. https://doi.org/10.1002/14356007.a27_049.
[40] B. Benstaali, D. Moussa, A. Addou, J.-L. Brisset, Plasma treatment of aqueous solutes: some chemical properties of a gliding arc in humid air, Eur. Phys. J. Appl. Phys. 4 (1998) 171–179.
[41] R. Cucciniello, A. Intiso, T. Siciliano, A.E. Palomares, J. Martínez-Triguero, J. L. Cerrillo, A. Proto, F. Rossi, Oxidative degradation of trichloroethylene over Fe2O3-doped mayenite: chlorine poisoning mitigation and improved catalytic performance, Catalysts 9 (2019) 747, https://doi.org/10.3390/catal9090747.
[42] J. Li, P. Zhao, S. Liu, SnO –MnO –TiO2 catalysts with high resistance to chlorine poisoning for low-temperature chlorobenzene oxidation, Appl. Catal. Gen. 482 (2014) 363–369.
[43] M. Li, F. Bi, Y. Xu, P. Hao, K. Xiang, Y. Zhang, S. Chen, J. Guo, X. Guo, W. Ding, Effect of residual chlorine on the catalytic performance of Co for CO oxidation, ACS Catal. 9 (2019) 11676–11684.
[44] M.H. Saad, Contribution à l'étude d'un réacteur plasma en post-déchrage N2-H2 appliqué à la stérilisation, (n.d.) 114.
[45] D. Mariotti, J. Patel, V. Švrček, P. Maguire, Plasma-liquid interactions at atmospheric pressure for nanomaterials synthesis and surface engineering: plasma-liquid interactions at atmospheric pressure…, Plasma Process. Polym. 9 (2012) 1074–1085.